Optics Letters

Micrometer-accuracy 2D displacement interferometer with plasmonic metasurface resonators

Chuanrui Guo,[1] Yuchao Zhang,[2] Matthew Klegseth,[1] Jie Gao,[2] and Genda Chen[1,*]

[1]Department of Civil, Architectural and Environmental Engineering, Missouri University of Science and Technology, Rolla, Missouri 65401, USA
[2]Department of Mechanical and Aerospace Engineering, Missouri University of Science and Technology, Rolla, Missouri 65401, USA
*Corresponding author: gchen@mst.edu

Received 9 October 2020; accepted 25 October 2020; posted 29 October 2020 (Doc. ID 412130); published 24 November 2020

In this Letter, a high-accuracy, two-dimensional displacement sensor is proposed, designed, and demonstrated based on the concept of an extrinsic Fabry–Perot Interferometer. The sensor is composed of two bundled single-mode optic fibers in parallel and two plasmonic metasurface resonators inscribed on a gold substrate via a focused ion beam. The fiber end surface and the metasurface are in parallel with a small cavity between. The cavity change or *Z*-component displacement is determined from the pattern of interference fringes. The *X*-component displacement, perpendicular to the *Z* component, is identified from wavelength-selective metasurface resonators, which possess unique resonant wavelengths due to different nanostructure designs. The sensor was calibrated with six displacements applied through a three-axis precision linear stage. Test results indicated that the proposed interferometer can measure displacements with a maximum error of 5.4 μm or 2.2%.

https://doi.org/10.1364/OL.412130

The extrinsic Fabry–Perot interferometer (EFPI) [1] has been widely used to measure various physical parameters such as strain [2,3], temperature [4], pressure [5], and displacement [6]. Compared to other fiber-based displacement sensors [7,8], it consists of two parallel reflective surfaces with a cavity along an optical fiber. When incident light is sent through the fiber, the two surfaces generate two reflection waves with time delay, inducing an interference fringe pattern in the output spectrum. The fringe pattern is a function of power intensity and the cavity length. Therefore, the cavity length can be determined from signal processing of the output spectrum. At the location of an EFPI, the two sides of an optic fiber are usually fixed on a substrate and aligned in a collimated capillary tube [1]. Such an application has three disadvantages. First, since the reflectivity of the fiber core is relatively low [5], the Q-factor or finesse of the optic fiber-based EFPI sensor is low. Secondly, the alignment and installation of the two fibers into the capillary tube are time-consuming and fragile due to the small (125 μm) diameter of the fiber. Thirdly, the optic fiber-based EFPI sensors can only measure cavity change in the direction of light propagation, limiting potential applications.

The plasmonic metasurface has received increasing attention in next-generation structural color filtering and printing applications [9–11]. Recently, various types of metasurfaces [12–14] in infrared range have been achieved to realize infrared perfect absorbers and optical index sensing. Since the wavelength range of a metasurface resonator contains a low attenuation band of the optic fiber, the combination of the optic fiber-based EFPI and the wavelength-selective metasurface resonator is feasible and promising for a two-dimensional (2D) displacement sensor design.

In this Letter, a 2D displacement sensor with high accuracy is proposed based on the EFPI and wavelength-selective plasmonic metasurfaces. The cavity change between the optic fiber end and the metasurface substrate is designated as a *Z*-component displacement. The metasurface arrays on the substrate with various resonant wavelengths are used to determine an *X*-component displacement. Compared with traditional EFPI sensors, the proposed interferometer has three main advantages. First, the gold metasurface substrate has higher reflectivity, which increases the Q-factor of the cavity and thus improves the sensor resolution. Secondly, the fabrication process of an optical fiber against a gold substrate is easier and more robust. Thirdly, the interferometer responds to two orthogonal components of a displacement.

Figure 1(a) shows a cross-shaped nanostructure unit cell located on the top layer of an Au−SiO_2−Au three-layer thin film. Multiple unit cells are arranged in a 2D square lattice, as shown in the scanning electron microscope (SEM) pictures [Fig. 1(b)], to form a plasmonic metasurface. Defined by the layer thicknesses of Au and SiO_2 films, the length and width (w) of the cross-shaped nanostructure, and the spatial period between two adjacent unit cells, the metasurface resonators are designed to have a resonant wavelength of 1460 to 1620 nm. Figure 2(a) presents the simulated reflection spectra of four metasurfaces with different widths, $w = 80$ nm ~ 140 nm, when the spatial period = 670 nm, cross length = 500 nm, top Au layer thickness = 55 nm, middle SiO_2 layer thickness = 145 nm, and bottom Au layer thickness = 200 nm. Design

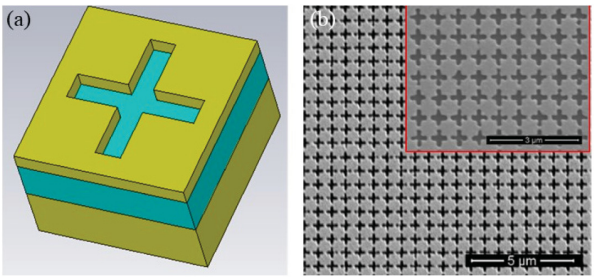

Fig. 1. Plasmonic metasurface (60 μm × 60 μm): (a) a cross-shaped unit cell with cross width w and (b) an SEM image with a close-up view.

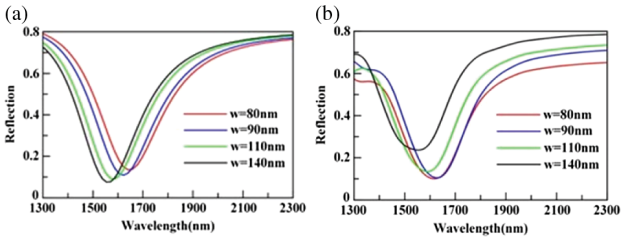

Fig. 2. Reflection spectra of metasurfaces with various cross widths w: (a) numerical simulations and (b) experimental results.

resonant wavelengths from 1550 to 1650 nm are achieved and verified by the numerical simulations.

The four designed metasurfaces were fabricated through thin film deposition of three layers of Au − SiO_2 −Au on a thick glass substrate with an electron–beam evaporator and focused ion beam (FIB) milling of the top Au thin film to form the plasmonic nanostructures directly. An SEM image of a 60 μm × 60 μm metasurface with cross $w = 90$ nm is shown in Fig. 1(b). Reflection spectra of the four metasurfaces, as shown in Fig. 2(b), were measured with a Fourier transform infrared spectrometer and a LN_2 cooled infrared detector. The measured reflection spectra clearly demonstrated wavelength-selective features of the metasurfaces with distinguishable resonant wavelengths, which agree well with the simulated results in Fig. 2(a). The differences in resonant wavelength, especially when $w < 100$ nm, are likely attributed to small discrepancies between the designed and the fabricated nanostructures.

The physical mechanism of the metasurface resonator was investigated in previous work [11]. A numerical simulation of the electromagnetic field distribution at resonant wavelength indicated that antiparallel currents were excited in the top and bottom gold films. A magnetic resonance was formed by the circulated currents and then interacted with the magnetic field of the incident light. Therefore, an enhanced magnetic field was established and confined in the middle SiO_2 dielectric layer. The electric field was mostly concentrated at the bottom side of the top gold layer. A strong electric dipole resonance was generated by the accumulated polarized positive and negative charges at the right and left corners of the cross-shaped aperture. The combination of the electric dipole and magnetic dipole resonance resulted in the matched impedance to free space and led to the selective resonant wavelength tuned by adjusting the width w of the cross-shaped nanostructure of the resonator.

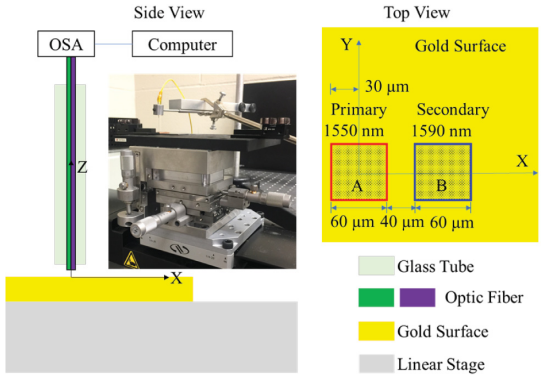

Fig. 3. Side and top views of the proposed interferometer with an insert on the test setup of a prototype.

A numerical simulation about the effect of the incident angle on the resonator was also conducted [11]. For TE polarization, the resonant wavelength was angle insensitive, but the reflection intensity increased with a larger incident angle, since the circulated currents cannot be driven effectively by the smaller horizontal magnetic field component at larger incident angles. For TM polarization, the resonant wavelength remained stable before $\theta = 20°$ and then slightly shifted to larger wavelengths due to the weak surface wave coupling between adjacent resonators. On the other hand, the reflection intensity remained 70% of the original value before $\theta = 80°$. Therefore, the incident angle should be controlled within 20° for sensor design to minimize the wavelength shift effect.

Figure 3 shows the design and test setup of an interferometer used to demonstrate its new concept. Two single-mode optic fibers (Corning SMF-28) are bundled in parallel and inserted into a capillary glass tube that is fixed slightly above the meta-surface substrate with the inscription of a primary resonator A (1550 nm) and a secondary resonator B (1590 nm). Each resonator has a unique resonant wavelength by adjusting the width w of the cross-shaped nanostructure, as shown in Fig. 1. The distance between the two resonators is 40 μm. The Cartesian coordinate system is set with its origin at the center of the primary resonator A, X axis and Y axis in the substrate surface, and Z axis along the fiber direction pointing upward. The substrate is fixed on a three-way linear stage (Newport 562) with 0.5 μm in displacement accuracy. The reflection spectrum of the interferometer is acquired by an optical interrogator (Micron Optics SI 255) and saved in a computer for further signal decoding.

Figure 4 illustrates the Z-direction displacement sensing principle of the proposed interferometer. When propagating through the fiber, incident light will be reflected at both the fiber end and the meta-surface substrate, and generate an interference fringe pattern. Although the reflected light from the metasurface is affected by its nanostructure design, the total intensity of the output signal can be approximated by [15]

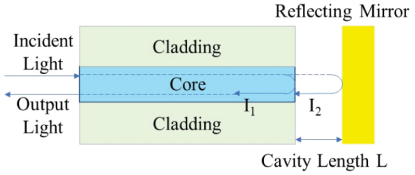

Fig. 4. Interference principle of the EFPI.

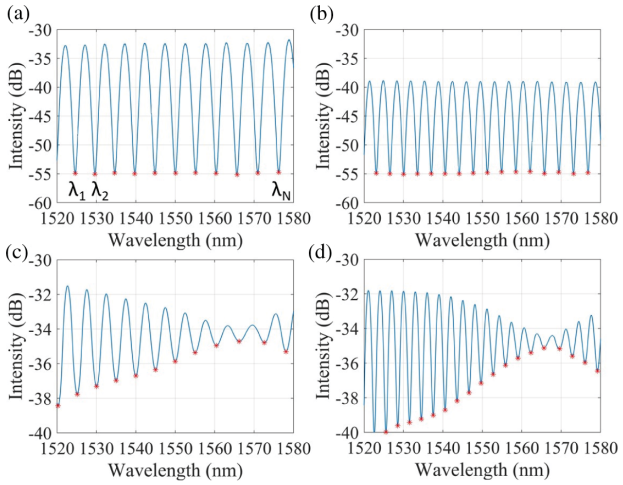

Fig. 5. Output spectra with an optical fiber perpendicular to a normal gold surface with cavity lengths of (a) 250 and (b) 300 μm, and the center of resonator B with cavity lengths of (c) 250 and (d) 300 μm.

$$I = I_1 + I_2 + 2\sqrt{I_1 I_2}\cos\left(\frac{4\pi n_0 L}{\lambda} + \varphi_0\right), \quad (1)$$

where I is the output intensity of the interferometer; I_1 and I_2 are the reflected light intensity at the fiber end surface and metasurface, respectively; L is the cavity length; $n_0 = 1$ (in air) is the refractive index of cavity medium; φ_0 is the initial phase; and λ is the wavelength of the reflected light. In the output spectrum of a traditional EFPI, as shown in Fig. 5(a), two adjacent valleys have the phase difference of 2π. Particularly,

$$\frac{4\pi L}{\lambda_1} - \frac{4\pi L}{\lambda_2} = 2\pi. \quad (2)$$

Therefore, the cavity length L can be determined by

$$L = \frac{\lambda_1 \lambda_2}{2(\lambda_1 - \lambda_2)}. \quad (3)$$

To validate the Z-direction displacement sensing, one optic fiber pointed at the gold surface and the resonator B with two different cavity lengths. When the optic fiber pointed at the gold surface, the output spectra of the sensor were recorded, as shown in Figs. 5(a) and 5(b). The wavelength at each marked valley in Figs. 5(a) and 5(b) was extracted from the spectra. Two adjacent wavelengths between λ_1 and λ_N were then used to obtain a cavity length from Eq. (3). Multiple cavity lengths determined were averaged as a high accuracy representation of the Z-component displacement applied. When the optic fiber pointed at the resonator, the output spectra of the sensor were recorded, as shown in Figs. 5(c) and 5(d). In this case, the EFPI interference pattern was coupled with the reflection spectrum of the resonator, but the marked valleys can still be identified from the coupled spectra to calculate the cavity length of the sensor. By comparing Figs. 5(a) and 5(b) with Figs. 5(c) and 5(d), there appears to be a weak interaction between the interferometric and the reflective spectra, which warrants further studies in the future.

Table 1 compares the set and measured values of cavity lengths in each case. The measured cavity lengths from the primary resonator B are slightly larger than from the gold surface

Table 1. Comparison of the Set and Measured Cavity Lengths

Fiber Position	Set Cavity Length (μm)	Measured Cavity Length (μm)	Error (%)
Gold Surface	250	252	0.8
	300	304	1.3
Resonator B	250	254	1.6
	300	306	2.0

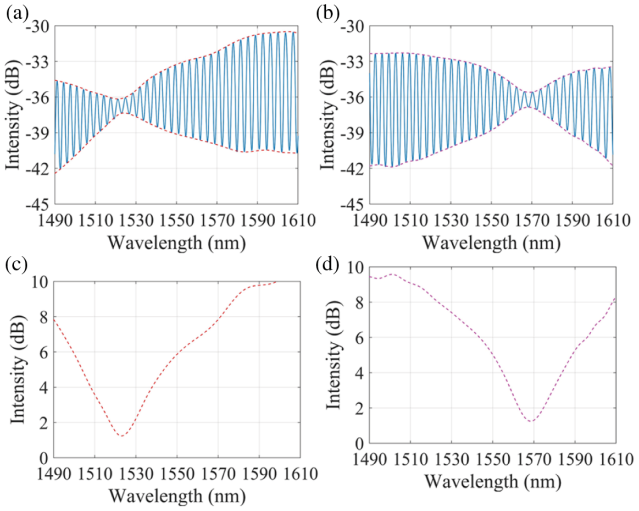

Fig. 6. (a) and (b) Output spectra of the interferometer when an optical fiber is placed directly above the centers of resonators A and B; (c) and (d) extracted reflection spectra.

with a maximum error of 2.0%. Thus, replacing the gold surface with the resonator changes little of the cavity length. Therefore, Eq. (3) can be used in both cases to acquire the cavity length accurately for the measurement of Z-component displacement.

For the X component displacement sensing, the reflection spectrum of a resonator is utilized. When the optic fiber pointed at the resonator A or B with a cavity length of 350 μm, the output spectrum of the sensor was recorded, as shown in Fig. 6(a) or 6(b). By connecting all the peak (or valley) points of each output spectrum, the upper (or lower) envelope of the spectrum was obtained as outlined in Figs. 6(a) or 6(b). The difference between the upper and lower envelopes was then calculated to determine the reflection spectrum associated with the resonator A or B. As shown in Figs. 6(c) and 6(d), the resonant wavelengths corresponding to each valley in the reflection spectra are 1523 and 1569 nm for resonators A and B, respectively, with a maximum error of 1.7% compared to the designed value.

Figure 7(a) shows the resonant wavelengths extracted from the reflection spectra of resonators A and B. When one fiber scans from the center to two edges of each resonator, the resonant wavelength decreases. This is because an increasing portion of the laser beam emitting from the fiber core is shot on the gold surface instead of the resonator. The size (60 μm in the X direction) of each resonator is in the same order of the diameter of a diverged light beam emitting from the fiber core to the metasurface, corresponding to a reduced light intensity of $1/e^2$ with Gaussian distribution, which is approximately 50 to 90 μm for a cavity length of 250 to 450 μm [16]. It seems that the resonant

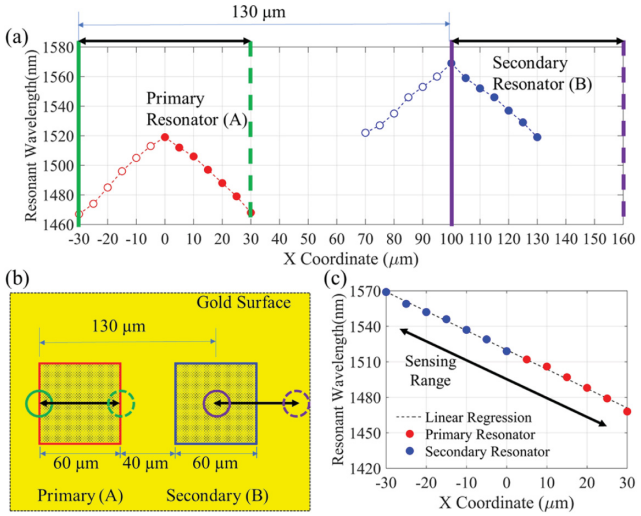

Fig. 7. (a) Resonant wavelengths extracted from an individual resonator A or B using one EFPI (250 μm cavity length), (b) a measurement scheme of two bundled sensors, and (c) combined resonant wavelength output versus X coordinate from the bundled sensors.

wavelength decreases linearly from the center to two edges in a symmetric manner.

To achieve monotonic displacement sensing in the X direction, two parallel optic fibers were bundled together with 130 μm in center-to-center spacing. As illustrated in Fig. 7(b) in the plan view, when one fiber (green) moved from the left edge to the center of the primary resonator A, the other fiber (purple) moved from the center to the right edge of the secondary resonator B. In this range, the resonant wavelength extracted from the purple fiber on the secondary resonator was higher than that from the green fiber. When the green fiber moved from the center to the right edge of the primary resonator A, the purple fiber moved to the gold surface with no reflection spectrum observed and thus a zero resonant wavelength assigned. In this Letter, the larger of the two resonant wavelengths from the two individual optic fibers is utilized in displacement sensing. As a result, the resonant wavelength extracted from the two fibers bundled together decreases linearly with the X coordinate, as shown in Fig. 7(c).

To investigate the feasibility and accuracy of the proposed interferometer in 2D coordinate sensing, the primary resonator A was scanned three times at cavity lengths of $L = 250$, 350, and 450 μm, respectively, at each of the two locations of $X = -10$ μm and $X = 10$ μm set by the precision three-way linear stage. The coordinates in X and Z directions were identified using the proposed method discussed above. Table 2 compares the set and measured (X, Z) coordinates with a maximum root–mean–square error of 5.4 μm or 2.2%.

In summary, a 2D displacement sensor with two parallel EFPIs bundled together with 130 μm spacing has been demonstrated to be successful in linear displacement measurement when two square wavelength-selective metasurface resonators (primary and secondary, each being 60 μm in the X direction) are spaced by 100 μm in center-to-center distance. The sensor is robust and has an accuracy of 5.4 μm or 2.2% over a dynamic range of −30 to +30 μm. The interference pattern and the low attenuation band of an output reflection spectrum can be decoupled to determine the cavity length and the resonant wavelength (then X coordinate) of a metasurface resonator. The changes in cavity length and X coordinate from the primary and secondary resonators can determine the Z component and X component of a displacement.

Table 2. Measurement Results of X and Z Coordinates

Position Case	Set (X, Z) Coordinate (μm)	Measured (X, Z) Coordinate (μm)	Error (%)
Scan 1-a	(–10,250)	(–8,252)	1.1
Scan 1-b	(10,250)	(15,252)	2.2
Scan 2-a	(–10,350)	(–10,346)	1.1
Scan 2-b	(10,350)	(12,347)	1.0
Scan 3-a	(–10,450)	(–13,453)	0.9
Scan 3-b	(10,450)	(10,447)	0.7

Funding. National Science Foundation (CMMI1235202, ECCS1653032); U.S. Department of Transportation (69A3551747126); U.S. Department of Energy (DE-AC02-06CH11357).

Acknowledgment. The Chinese Scholarship Council (CSC) provided scholarship for the first author to study abroad. This Letter was performed in part at the Center for Nanoscale Materials, a U.S. Department of Energy, Office of Science, Office of Basic Energy Sciences User Facility.

Disclosures. The authors declare no conflicts of interest.

REFERENCES

1. K. A. Murphy, M. F. Gunther, A. M. Vengsarkar, and R. O. Claus, Opt. Lett. **16**, 273 (1991).
2. T. Wang, S. Zheng, and Z. Yang, Sens. Actuators, A **69**, 134 (1998).
3. J. Leng and A. Asundi, Sens. Actuators, A **103**, 330 (2003).
4. X. Wen, T. Ning, Y. Bai, C. Li, J. Li, and C. Zhang, Opt. Express **23**, 11526 (2015).
5. F. Xu, D. Ren, X. Shi, C. Li, W. Lu, L. Lu, L. Lu, and B. Yu, Opt. Lett. **37**, 133 (2012).
6. X. Zhou and Q. Yu, IEEE Sens. J. **11**, 1602 (2011).
7. S. Tao, X. Dong, and B. Lai, Opt. Commun. **372**, 44 (2016).
8. Q. Wu, Y. Semenova, P. Wang, A. M. Hatta, and G. Farrell, Meas. Sci. Technol. **22**, 025203 (2011).
9. Z. Li, W. Wang, D. Rosenmann, D. A. Czaplewski, X. Yang, and J. Gao, Opt. Express **24**, 20472 (2016).
10. Y. K. R. Wu, A. E. Hollowell, C. Zhang, and L. Jay Guo, Sci. Rep. **3**, 1194 (2013).
11. F. Cheng, J. Gao, S. T. Luk, and X. Yang, Sci. Rep. **5**, 11045 (2015).
12. Z. Li, X. Yang, D. A. Czaplewski, L. Stan, and J. Gao, Opt. Express **26**, 5616 (2018).
13. F. Cheng, X. Yang, and J. Gao, Opt. Lett. **39**, 3185 (2014).
14. Y. Yao, R. Shankar, M. A. Kats, Y. Song, J. Kong, M. Loncar, and F. Capasso, Nano Lett. **14**, 6526 (2014).
15. Y. Huang, T. Wei, Z. Zhou, Y. Zhang, G. Chen, and H. Xiao, Meas. Sci. Technol. **21**, 105308 (2010).
16. A. M. Kowalevicz and F. Bucholtz, Beam divergence from an SMF-28 optical fiber, Naval Research Laboratory Report No. NRL/MR/5650–06-8996 (2006).